

## RESEARCH ARTICLE OPEN ACCESS

# Single-Ion Conductive Bacterial Cellulose Membrane Towards High Performance Lithium-Oxygen Batteries

Aqiang Wu<sup>1</sup> | Mingxing Wang<sup>1</sup> | Yaming Pang<sup>1</sup> | Xinyu Li<sup>2</sup> | Xiangqun Zhuge<sup>1</sup> | Zhihong Luo<sup>3</sup> | Guogang Ren<sup>4</sup> | Kun Luo<sup>1</sup> | Yurong Ren<sup>1</sup> | Dan Liu<sup>5</sup> | Weiwei Lei<sup>5</sup> | Jianwei Lu<sup>5</sup> 

<sup>1</sup>Jiangsu Province Engineering Research Centre of Intelligent Manufacturing Technology for the New Energy Vehicle Power Battery, Changzhou University, Changzhou, P. R. China | <sup>2</sup>Department of Chemical Engineering and Materials Science, University of Minnesota, Minneapolis, Minnesota, USA | <sup>3</sup>College of Materials Science and Engineering, Guilin University of Technology, Guilin, P. R. China | <sup>4</sup>University of Hertfordshire, Hatfield, Hertfordshire, UK | <sup>5</sup>School of Science, STEM College, RMIT University, Melbourne, Victoria, Australia

**Correspondence:** Kun Luo ([luokun@cczu.edu.cn](mailto:luokun@cczu.edu.cn)) | Jianwei Lu ([S4126654@student.rmit.edu.au](mailto:S4126654@student.rmit.edu.au))

**Received:** 3 January 2025 | **Revised:** 14 March 2025 | **Accepted:** 8 April 2025

**Funding:** This study was supported by the National Natural Science Foundation of China (Nos. 51874051 and 52111530139), the Australian Research Council Discovery Program (DP220103416), and Australian Research Council Future Fellowships (FT200100730 and FT210100804).

**Keywords:** bacterial cellulose membranes | lithium-oxygen batteries | separators | single ion conductivity

## ABSTRACT

Bacterial cellulose (BC) as a natural polymer possessing ultrafine nanofibrous network and high crystallinity, leading to its remarkable tensile strength, moisture retention and natural degradability. In this study, we revealed that this BC membrane has excellent affinity to organic electrolyte, high ionic conductivity and inherent ion selectivity as well. Due to its ability of migrating lithium ions and suppressing the shuttling of anions across the membranes, it is deemed as available model for iodide-assisted lithium-oxygen batteries (LOBs). The cycle life of the LOBs significantly extends from 74 rounds to 341 rounds at 1.0 A g<sup>-1</sup> with a fixed capacity of 1000 mAh g<sup>-1</sup>, when replacing glass fiber (GF) by BC membrane. More importantly, the rate performance improves significantly from 42 to 36 cycles to 215 and 116 cycles after equipping with the BC membrane at 3.0 and 5.0 A g<sup>-1</sup>. Surprisingly, the full discharge capacity dramatically enhanced by ca. eight times from 4,163 mAh g<sup>-1</sup> (GF) to 32,310 mAh g<sup>-1</sup> (BC). Benefited from the convenient biosynthesis, cost-effectiveness and high chemical-thermal stability, these qualities of the BC membrane accelerate the development and make it more viable for application in advancing next-generation environmentally friendly LOBs technology with high energy density.

## 1 | Introduction

As a prospective candidate to substitute widely used lithium-ion batteries (LIBs), the lithium-oxygen batteries (LOBs) owns a ultrahigh theoretical energy density up to 3500 Wh kg<sup>-1</sup> [1], however, it still faces technological challenges including poor cycle stability, low coulomb efficiency and cathode passivation, etc [2]. In discharging, the formation of Li<sub>2</sub>O<sub>2</sub> in oxygen reduction reaction (ORR) often accompanies with superoxide intermediates (such as O<sub>2</sub><sup>-</sup>, LiO<sub>2</sub>, etc.), which tend to be

oxidative to the organic electrolyte and Li anode [3]. In recharging, the discharge product Li<sub>2</sub>O<sub>2</sub> is insulative with a large band gap (~4.9 eV), which impedes electron transfer and ion diffusion and leads to sluggish kinetics of oxygen evolution reaction (OER) [3, 4]. Redox mediators (RMs) including LiI [5], tetrathiafulvalene (TTF) [6], 2,5-di-tert-butyl-1,4-benzoquinone (DBBQ) [7], 2,2,6,6-tetramethylpiperidinyloxy (TEMPO) and iron phthalocyanine (FePc) [8], have shown advantage in ameliorating sluggish ORR and OER kinetics [9], which act as mobile charge carriers in the electrolyte solution and facilitate

Aqiang Wu and Mingxing Wang are first authors.

This is an open access article under the terms of the [Creative Commons Attribution](https://creativecommons.org/licenses/by/4.0/) License, which permits use, distribution and reproduction in any medium, provided the original work is properly cited.

© 2025 The Author(s). *Battery Energy* published by Xijing University and John Wiley & Sons Australia, Ltd.

### Summary

- Bacterial cellulous (BC) membranes could be utilized as separator after purification.
- BC membranes exhibited high  $\text{Li}^+$  conductivity and minimum permeation of  $\text{I}^-$  and  $\text{I}_3^-$ .
- BC separators significantly enhanced the LiI-mediated lithium-oxygen batteries.
- BC separators are cost-effective with high thermal and chemical stability.

electron transfer at the cathode/electrolyte/ $\text{O}_2$  and cathode/ $\text{Li}_2\text{O}_2$  interfaces [10]. Other RMs, such as 10-methyl-10H-phenothiazine (MPT) [11], dimethylphenazine (DMPZ) [12], Fe(heme) and  $\text{LiNO}_3$  [13], were also reported to accelerate the kinetics of LOBs reactions. Among them, LiI was frequently employed, but the corresponding catalytic mechanism remained unclear [14].

Due to the soluble nature of RMs, the oxidized RMs can easily diffuse in the electrolyte and induce deterioration of Li anodes [15], and meanwhile some undesirable species originated from Li-metal corrosion may migrate to the detriment of cathode processes as well, termed as “shuttling effect” [3]. The straightforward method is to enhance the ionic selectivity of battery separators. Wu et al used the  $\text{Li}^+$ -Nafion separator to prohibit the crossover of RMs towards Li-metal anode, where the charge overpotential was low to 0.24 V and shuttling problems of LOBs were effectively avoided [16]. Modification of a glass fiber separator with negatively charged polymer was also reported to mitigate the migration of the oxidized RM DMPZ by coulombic interactions [12]. In our previous work, sulfonated poly(vinylidene fluoride) modified with an ionic liquid was synthesized as a single-ion conductive separator, which owned high conductivity of  $\text{Li}^+$  and low passthrough of anions, and effectively enhanced the performance of LiI-assisted LOBs [17]. Chen et al. further proposed a composite NPG membrane to suppress the shuttling effect in LiI assisted LOBs, where the O atoms in PEO, the sulfonic acid groups in Nafion and the graphene skeleton formed a dense network barrier to offer single-ion conductivity, and resulted in an ultralong cycle life (472 cycles) at  $500 \text{ mA g}^{-1}$  with a cutoff capacity of  $500 \text{ mAh g}^{-1}$  [18]. MOF-based separators were also developed to restrain the shuttling of dual RMs and significantly stabilized the LOBs [19].

It is of engineering significance to develop a short process for cost-effective fabrication of robust single-ion separators. The inherent biodegradability of bacterial cellulose (BC) membranes, coupled with their tunable physicochemical characteristics (e.g., porosity

modulation via biosynthesis control and surface functionalization through hydroxyl-group modification), renders them a sustainable and high-performance alternative to conventional polyolefin separators in LIBs system [20]. Attempts have been made to apply BC membrane in lithium-ion and lithium-sulfur batteries [21]. In this study, we revealed the excellent affinity to DMSO electrolyte and high single-ion conductivity in organic electrolyte for the first time, which brought much better lithium ions transference and suppressed the shuttling of  $\text{I}^-$  and  $\text{I}_3^-$  across the BC membrane. The life span of LOBs exhibited a marked prolongation, and the rate performance and full discharge capacity also improved significantly.

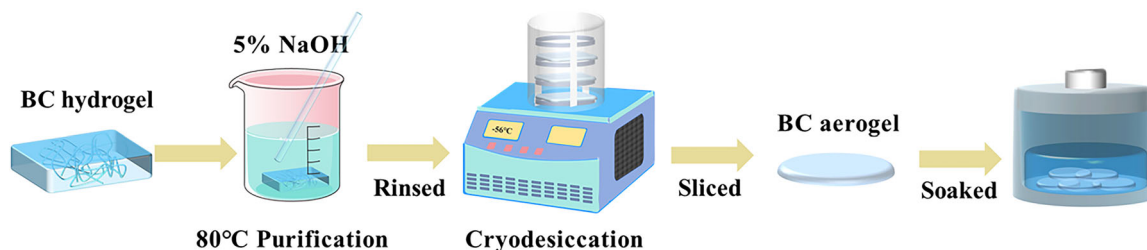
## 2 | Experimental

### 2.1 | Materials and Chemicals

Bacterial cellulose (BC) hydrogels (1, 3 and 5 mm in thickness) were purchased by Chihong Technology Co. Ltd. Sodium hydroxide (NaOH) was purchased from Sinopharm Chemical Reagent Co. Ltd. Dimethyl sulfoxide (DMSO, 99.9%), propylene carbonate (PC, 99.7%), lithium perchlorate ( $\text{LiClO}_4$ , 99.99%) and lithium iodide (LiI, 99.99%) were bought from Sigma-Aldrich. Multiwalled carbon nanotubes (MWNTs, 95%, 10–30  $\mu\text{m}$ ) was bought from Xfnano. Glass fiber (thickness = 780  $\mu\text{m}$ , GF, Whatman) and carbon paper (TGP-H-060, relative hydrophilic, Toray) were purchased from Siner Technology Co. Ltd.  $\text{LiClO}_4$  and LiI were dried in vacuum oven at  $110^\circ\text{C}$  for 10 h, and then prepared  $1.0 \text{ mol L}^{-1}$   $\text{LiClO}_4/\text{DMSO}$  electrolyte (anolyte) and  $0.05 \text{ mol L}^{-1}$  LiI/ $1.0 \text{ mol L}^{-1}$   $\text{LiClO}_4/\text{DMSO}$  electrolyte (catholyte). The activated molecular sieve (4 Å, Sigma-Aldrich) was added to the electrolyte and de-watered for 2 weeks before use. Lithium foils (15.6\*0.45 mm, Dodochem) were immersed in  $0.1 \text{ mol L}^{-1}$   $\text{LiClO}_4/\text{PC}$  solution for 3 days before use.

### 2.2 | Preparation of BC Membrane

Scheme 1 demonstrates the preparation of the BC membrane. The as-received BC hydrogels possess a gel of interconnected BC nanofiber network with 99% of water. It was necessary to purify the precursor of BC membrane before use as a battery separator, which was firstly treated in 5% NaOH solution at  $80^\circ\text{C}$  for 6 h to remove the proteins inside. Then, the BC membrane was taken out and rinsed with deionized water, and was stored in aqueous solution at  $4^\circ\text{C}$ , followed with freeze-drying for 24 h to obtain the BC membrane. BC membrane with different thicknesses were cut into the same diameter of 18 mm, named as BC-1, BC-3 and BC-5. Subsequently, BC membrane



**SCHEME 1** | Manufacturing of the Bacterial Cellulose (BC) membrane.

were employed as separators in LOBs after soaking with  $1 \text{ mol L}^{-1} \text{ LiClO}_4/\text{DMSO}$  electrolyte. Before assembling into the cells, the BC-1, BC-3, and BC-5 membranes thickness were 1, 3, and 5 mm, respectively. After sealing, the actual thickness of BC-1, BC-3 and BC-5 inside the battery were 70, 110 and  $160 \mu\text{m}$ , respectively.

### 2.3 | Construction and Testing of LOBs

Twenty micrograms of MWNTs were added into 40 mL of ethanol, which were dispersed by ultrasonic stirring, and the yielded slurry was sprayed uniformly on a carbon paper at the loading of  $0.1 \text{ mg cm}^{-2}$ . After vacuum drying at  $80^\circ\text{C}$  for 12 h, the carbon paper was cut into square sheets in size of  $1.0 \text{ cm} \times 1.0 \text{ cm}$ , which were used as cathodes. The assembly of coin cells (CR2032 type, positive shell with holes) were carried out in a glove box with high-purity argon (99.999%) (Nanjing Jiumen Automation Technology Co. Ltd.,  $\text{H}_2\text{O} < 0.1 \text{ ppm}$ ,  $\text{O}_2 < 0.1 \text{ ppm}$ ), in the following order: anode shell - stainless steel - Li plate - a BC membrane (Soaked in anolyte beforehand) - a GF - injection of catholyte - cathode - elastic plate - cathode shell. The coin cells were kept in the glovebox overnight after sealing before performance testing.

The LOB test was carried out in pure oxygen ( $\geq 99.9\%$ ), and the ambient temperature was  $25^\circ\text{C}$ . The batteries were tested at the current density of  $1000 \text{ mA g}^{-1}$  with a fixed capacity of  $1000 \text{ mAh g}^{-1}$  (based on the loading mass of MWNTs), and the cut-off voltages were set up at 2.0 V for discharging and 4.5 V for charging. The rate performance was tested at the fixed capacity of  $1000 \text{ mAh g}^{-1}$ , in which the current density varied to 3000 and  $5000 \text{ mA g}^{-1}$ , respectively. As for the full discharge test, the

current was 0.1 mA, the cut-off voltage was 2.0 V, following the equation: Full discharge capacity = (total discharge time\*current)/(cathode area\*MWNTs loading). Li||Li symmetric batteries were used to study the effect of BC membrane on the stability of Li anodes. The applied voltage ranged from  $-1.5$  to 1.5 V, and the current was  $0.1 \text{ mA cm}^{-2}$ , and the charging/discharging time is 1 h, respectively.

### 2.4 | Characterizations

Morphological and structural analyses were performed by a scanning electron microscope (SEM, Phenom LE, Thermo Fisher Scientific). X-ray photoelectron spectroscopy (XPS) (Thermo ESCALAB 250XI), X-ray diffractometer (XRD, Bruker D8 Advance diffractometer, Cu-K $\alpha$ ), Raman spectrometer (532 nm, DXR2, Thermo), and Fourier transform infrared spectroscopy (FTIR, Thermo Scientific Nicolet iS5) were also used to characterize the samples. Electrochemical workstation (CHI660E, Shanghai Morning China Instrument Co. Ltd.) was used to carry out electrochemical impedance spectroscopy (EIS) and Cyclic voltammetry (CV) analysis.

## 3 | Results and Discussion

### 3.1 | Characterizations of the BC Membrane

In comparison to the conventional GF shown in Figure 1a, the BC membrane (Figure 1d displays a much denser texture in SEM image, which consists of three-dimensional interconnected nanofibers. FTIR and XRD were applied to investigate the structures and chemical composition of the BC membrane. FTIR

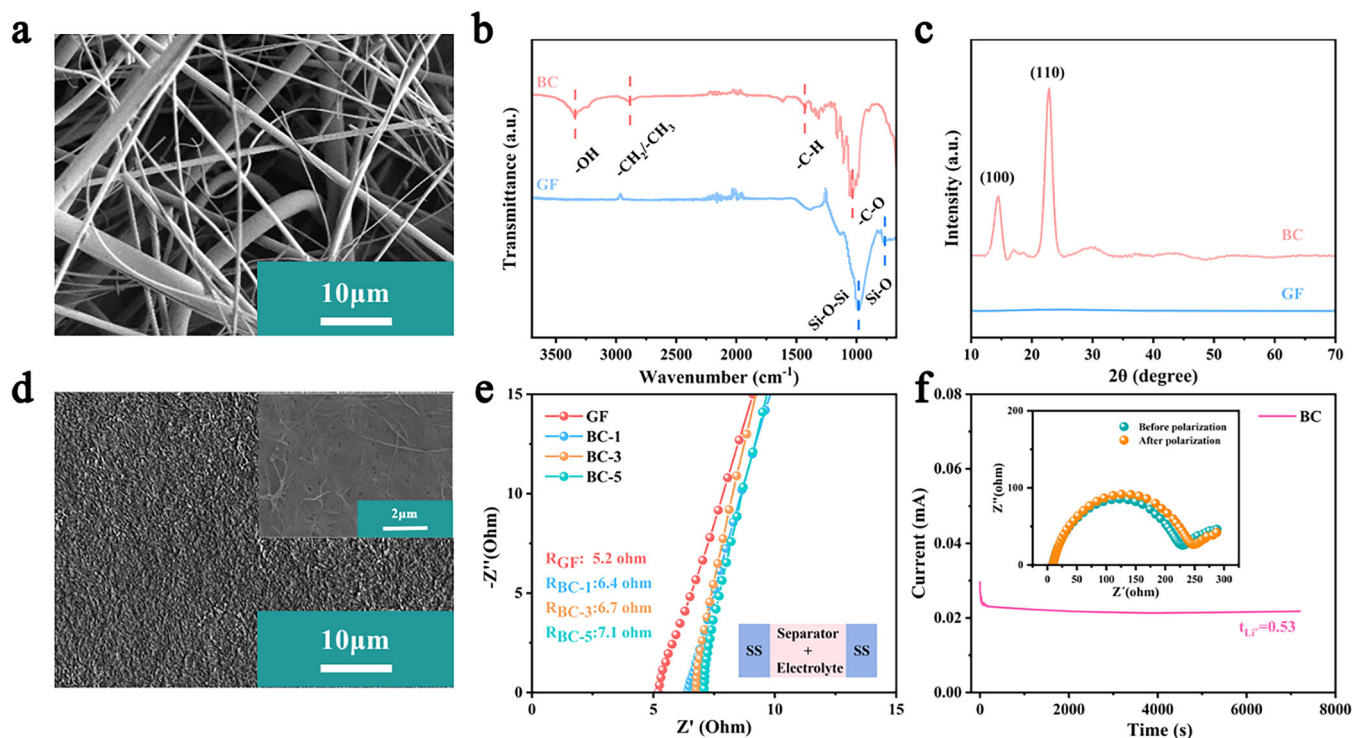


**FIGURE 1** | SEM images of the (a) GF and (d) BC membrane. (b) FTIR, (c) XRD and (e) EIS analyses in a SS||SS symmetric cell of the BC and GFs. (f)  $\text{Li}^+$  transference number of the BC membrane tested in a Li||Li symmetric cell.

analysis was shown in Figure 1b, the BC membrane exhibits the characteristic peaks of  $-\text{OH}$  stretching vibration at  $3346\text{ cm}^{-1}$ ,  $-\text{CH}_3/-\text{CH}_2$  stretching vibration at  $2883\text{ cm}^{-1}$ ,  $\text{C}-\text{H}$  bending at  $1431\text{ cm}^{-1}$  and  $\text{C}-\text{O}$  stretching vibration at  $1034\text{ cm}^{-1}$  [22]. These polar functional groups could clearly enhance the affinity of lithium ions to electrolyte and lithium ion migration. Furthermore, the FTIR of GF displays the symmetric stretching vibration of  $\text{Si}-\text{O}$  at  $781\text{ cm}^{-1}$  and the asymmetric stretching vibration of  $\text{Si}-\text{O}-\text{Si}$  at  $985\text{ cm}^{-1}$  [23]. XRD analysis in Figure 1c manifests two strong peaks at  $2\theta$  of  $14.5^\circ$  and  $22.5^\circ$ , corresponding to crystal plane (100), and (110), respectively, indicating the typical  $\alpha$  crystalline cellulose [21, 24]. In contrast, the GFs displayed an outstanding amorphous crystal structure.

As separator candidates, the physical and chemical properties of the BC were systematically evaluated to reconfirm it is suitable for LOBs. The thermal shrinkage pictures of the separators were given to investigate the thermal stability with different temperatures, as shown in Supporting Information S1: Figure 1. BC membrane exhibited comparable dimensional stability, high thermal stability and high safety in extreme conditions with the inorganic GF at elevated temperatures of  $100^\circ\text{C}$  and  $200^\circ\text{C}$ , respectively. As comparison, another polymer membrane of polyvinylidene fluoride (PVDF) manifests apparent size shrinkage with the increase of temperature, implying the possible shortcut between anode and cathode at high temperature. The BC membrane was then put in a liquid electrolyte for a few days to test the chemical stability. Supporting Information S1: Figure 2 depicts the chemical stability of liquid electrolyte for the BC membrane, where the BC membrane with saturated absorbed electrolyte maintained its topography for up to 40 days without visible change. Supporting Information S1: Figure 3 displays the contact angle measurements, where the GF exhibits excellent affinity to water and DMSO with the contact angles of  $0^\circ$ , and the contact angles of the BC membrane are  $27^\circ$  to water and  $14^\circ$  to DMSO, which are also suitable as a battery separator. In addition, the BC membrane exhibited good mechanical strength and flexibility, owing to its compact texture of 3D interconnected nanofibrous networks.

The superior electrolyte uptake and special hierarchical channels structure of BC membrane are the key reason to enhance interfacial compatibility and ionic conductivity. Indeed, BC-3 displayed the ionic conductivity of  $6.4\text{ mS cm}^{-1}$  (ref. Section S1.1 in Supporting Information) from EIS, as shown in Figure 1e and Supporting Information S1: Figure 4. The ionic conductivity of BC-1 is not much higher than that of BC-3. Its value is in the top rank in comparison to the data in previous reports (Supporting Information S1: Table 2). Li-symmetric cells were constructed, and their lithium-ion transference number ( $t_{\text{Li}^+}$ ) was estimated by DC polarization and EIS measurements (ref. Section S1.2 in Supporting Information). Figure 1f displays the corresponding chronoamperometry profiles and Nyquist plots, where the BC membrane exhibits a high  $\text{Li}^+$  ions transference number ( $t_{\text{Li}^+}$ ) of 0.53 in comparison to previous literatures (Supporting Information S1: Table 2). The high transference number can be assigned to the strong interactions between the oxygenated functional groups on the BC chains and the  $\text{Li}^+$  ions, which provide great amount of transportation routes for  $\text{Li}^+$  ions.

It is widely accepted that the  $\text{Li}^+$  ions are weakly associated with some polymer functional groups, and easily dissociate by solvation

in the organic electrolyte [25]. To understand the high  $\text{Li}^+$  single-ion conductivity of the BC membrane, density functional theory (DFT) calculations were performed to simulate the interaction between  $\text{Li}^+$  and bacterial cellulose network. The optimized structure of cellulose and its interaction with  $\text{Li}^+$  is depicted in Figure 2a. Clearly, the cellulose displays a 1D molecular chain with oxygen-rich polar functional groups, for example hydroxyl. The adsorption energy of  $\text{Li}^+$  on the cellulose is calculated as  $-1.60\text{ eV}$ . The low adsorption energy on the BC promotes rapid  $\text{Li}^+$  transport. The diffusion behavior of  $\text{Li}^+$  in the BC membrane was studied by using the CI-NEB method. In Figure 2b and Supporting Information S1: Figure 5, migration pathway for  $\text{Li}^+$  along a single 1D bacterial cellulose chain is considered. As shown in Figure 2c, the migration pathway displays low diffusion barriers of just  $0.185\text{ eV}$ , and the lower diffusion barrier in the cellulose means a higher diffusion rate, which is favorable to improve the ionic conductivity of the BC membrane.

More importantly, the BC membrane was evidenced to possess ionic selectivity, which can transfer  $\text{Li}^+$  ions and suppresses the shuttling of anions across the membrane, i.e., with lithium single-ion conductivity. Supporting Information S1: Figures 6 and 7 demonstrate the permeability experiments in a H-type electrolytic cell separated with a BC membrane or a conventional GF in the middle. Involving the environmental effect during battery charging/discharging processes, the enhancement originated from electric field to the transfer of  $\text{I}^-$  and  $\text{I}_3^-$  across the BC membrane was investigated as well. It is seen in the insets of Supporting Information S1: Figure 6a that  $\text{I}^-$  transferred across the GF only after 50 min, and the BC membrane could block the permeation of  $\text{I}^-$  for no less than 20 days (see Supporting Information S1: Figure 6b), which took effect even when the diffusion of  $\text{I}^-$  was driven by an electric field (see Supporting Information S1: Figure 6c). Supporting Information S1: Figure 7 displays the same results, where the BC membrane effectively suppressed the permeation of  $\text{I}_3^-$  even driven by an electric field. The ionic selectivity can be originated from the electrostatic interaction between the oxygen-rich groups on bacterial cellulose and anions, and the hydrogen bond with the hydroxyl group on bacterial cellulose also inhibits the transference of some specific anions.

### 3.2 | Performance of the LOB With the BC Membrane

In iodide-assisted LOBs, the shuttling of the oxidized RM ( $\text{I}_3^-$ , etc.) and other harmful species (moisture, oxidative species and decomposed products of electrolyte) can corrupt Li anodes, and the diffusion of RM ( $\text{I}^-$ ) also weakens the role of RM in cathode reactions. Therefore, impermeable separators with  $\text{Li}^+$  single-ion conductivity are preferable for the iodide-assisted LOBs. First, the ion diffusion of the BC membrane was tested by EIS measurements. As shown in Supporting Information S1: Figures 8 and 9 and Supporting Information S1: Table 1, the charge transfer resistance ( $R_{\text{ct}}$ ) of the BC-3 cell ( $146.2\ \Omega$ ) separator meets the requirements of LOBs cycle. Figure 3a shows the LOB with the GF can only run 74 cycles at the current density of  $1000\text{ mA g}^{-1}$  with the fixed specific capacity of  $1000\text{ mAh g}^{-1}$ . In contrast, in typical LOB system, with the BC-3 membrane in Figure 3b exhibits apparently lower charge potentials in the first 200 cycles, ended up with a long lifespan of 341 cycles. The LOBs

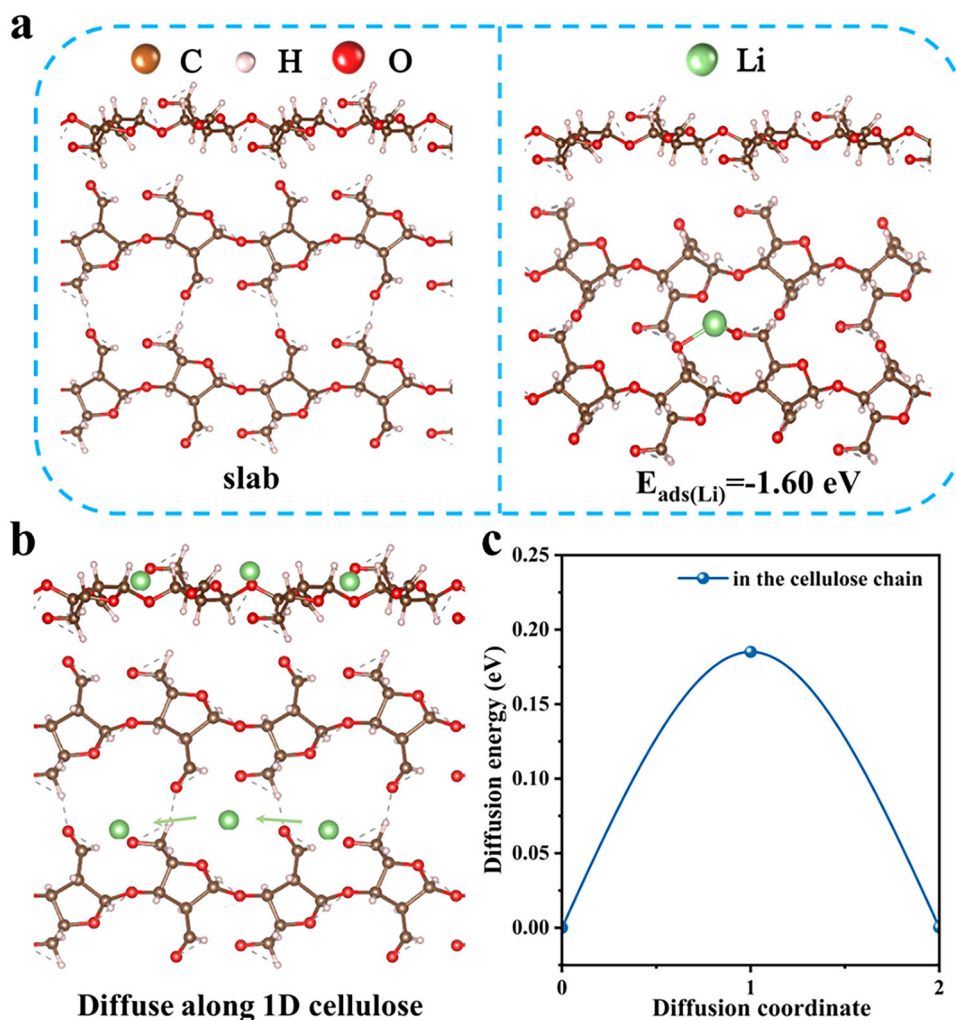


**FIGURE 2** | Calculated interaction of  $\text{Li}^+$  with bacterial cellulose and the corresponding optimized structures: (a) Optimized structures of  $\text{Li}^+$  adsorbed on bacterial cellulose. (b) Migration pathways of  $\text{Li}^+$ . (c) Corresponding diffusion energy profiles of  $\text{Li}^+$  on the bacterial cellulose.

with BC-1 and BC-5 membranes achieved only 241 and 276 cycles, respectively (Supporting Information S1: Figure 10a,b). While initial impedance values for BC-1 and BC-3 are comparable (Figure 1e), the stability of interfacial impedance during cycling is critical. BC-3 with stable charge/discharge profiles (Figure 3b) suggests minimal impedance growth over cycles. Meanwhile, BC-1 with faster capacity decay (Supporting Information S1: Figure 10a) implies accelerated interfacial degradation. This demonstrates that the BC-3 membrane effectively enhances charge transfer kinetics, and reduces polarization, ensuring long-term interfacial stability. Figure 3c displays the testing of full discharge capacity of the LOBs, in which the cell equipped with the GF displayed the full discharge capacity of  $4163 \text{ mAh g}^{-1}$ , and the value for the one with the BC-3 membrane is up to  $32,310 \text{ mAh g}^{-1}$ , about eight times larger than the cell with the GF. When comparing with BC-1 membrane ( $25,554 \text{ mAh g}^{-1}$ ) and BC-5 membrane ( $29,461 \text{ mAh g}^{-1}$ ) (see Supporting Information S1: Figure 10c), BC-3 membrane showed a substantial advantage. This confers its unique ability to facilitate efficient oxygen diffusion, lithium-ion transport, and  $\text{Li}_2\text{O}_2$  deposition, via its optimized surface properties. Besides, the full discharge capacity of the LOB with the GF and BC-3 membrane operated in argon atmosphere is only 7 and  $18 \text{ mAh g}^{-1}$ , as shown in Supporting Information S1: Figure 10d, demonstrating that the full-discharge capacity of the LOB with the BC membrane can be

assigned to ORR. Figure 3d displays the trends of discharge and charge potentials for the cells with the GF and BC-3 membrane, from which the failure of the former is due to the decrease of discharge potential associated with the depletion of Li anode, and the latter exhibits the increase of charge potential with battery cycling, attributed to the passivation of cathode by discharge product accumulation. Figure 3e illustrates the rate performance of the LOBs the GF and BC-3 membrane, in which the specific capacity of  $1000 \text{ mA g}^{-1}$  remained stable, and the current density varied to 3000 and  $5000 \text{ mA g}^{-1}$ . Correspondingly, the LOB with the BC-3 membrane could cycle for 215 and 116 rounds, while the LOB with the GF could only run only 42 and 36 rounds, respectively, i.e., the use of the BC-3 membrane brought with nearly 4~5 times increase in rate performance.

Based on the comparative evaluation of electrochemical impedance, conductivity, and battery cycling performance among BC membranes, we found BC-3 membrane demonstrated superior comprehensive properties, which implied the BC-3 simplified as BC membrane was suitable as separator.

In the symmetric cell test (Supporting Information S1: Figure 11), the cell with GF short circuits at 246 h, due to the accumulation and penetration of lithium dendrites. In contrast,

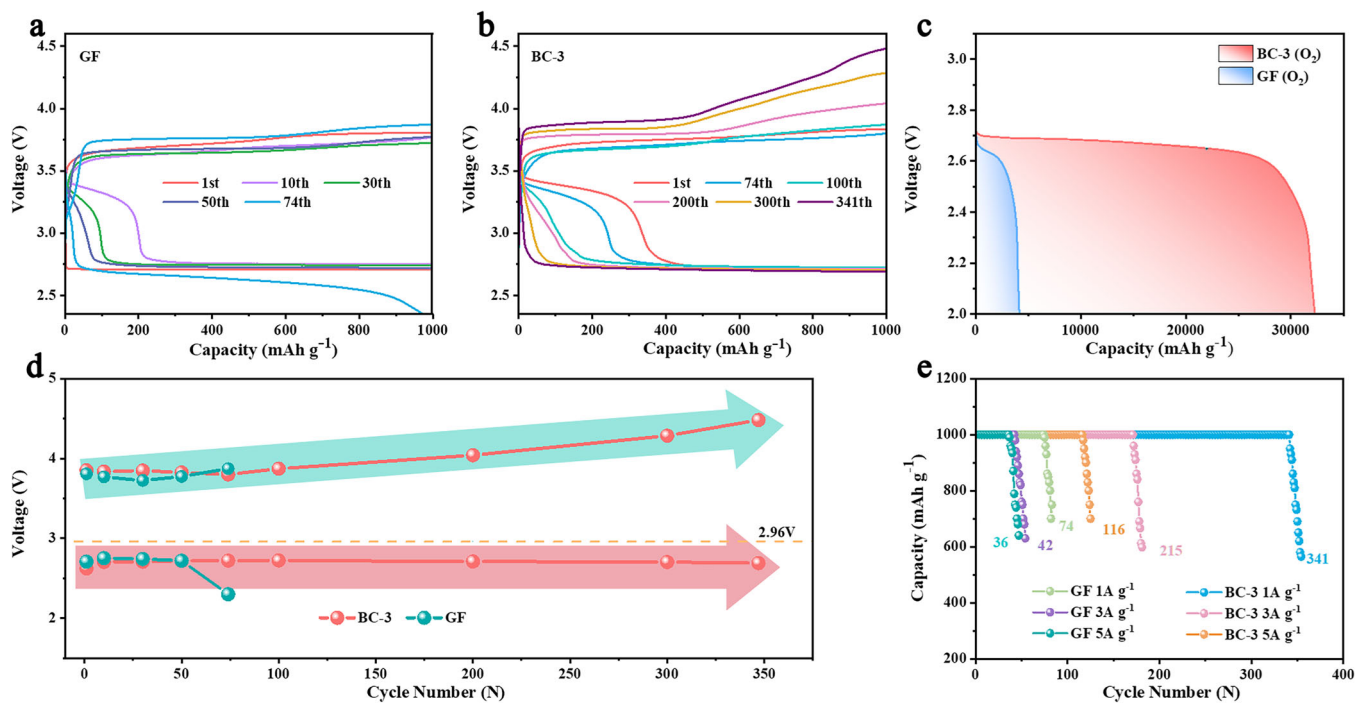


**FIGURE 3** | Cyclability of LOBs with the (a) GF and (b) BC-3 membranes. (c) Full discharge capacity with the GF and BC-3 membranes. (d) Discharge/charge open circuit potentials with GF and BC-3 membranes. (e) Rate performance with the GF and BC-3 membranes.

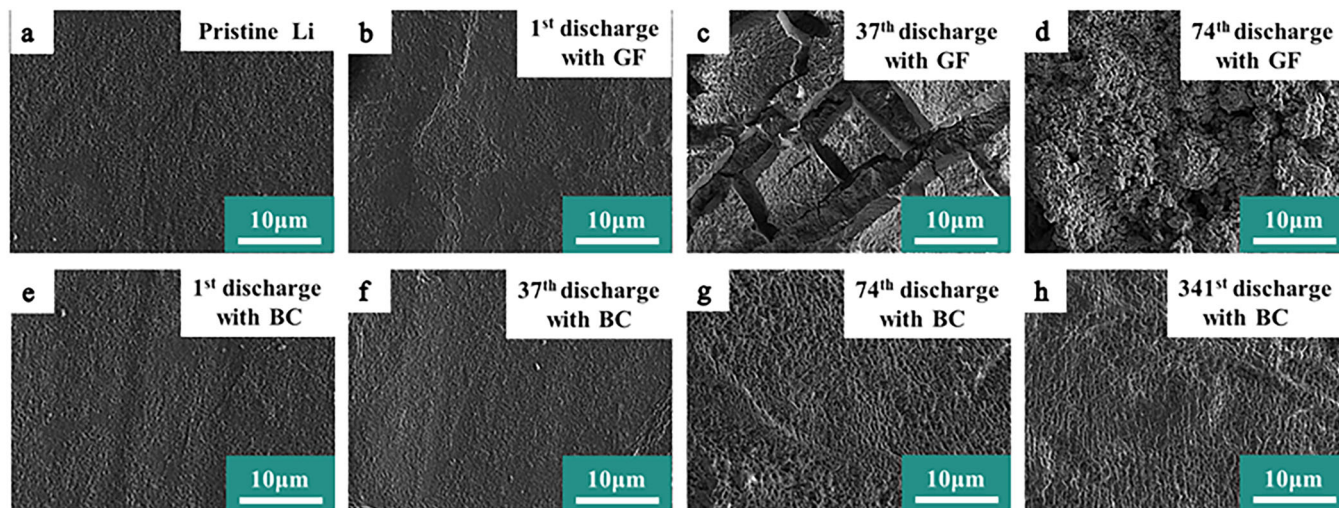


**FIGURE 4** | (a) Surface images of the pristine Li anode. (b–d) After the 1st, 37th and 60th discharges in the iodide-assisted LOB with the GF. (e–h) The Li anode in the iodide-assisted cell with the BC membrane after the 1st discharges, 37th discharges, 74th discharges and 341th discharges.

the BC cell can run up to 776 h with the low potential difference (0.37 V). By the symmetric cell test, BC is able to facilitate the stable plating and stripping of lithium.

### 3.3 | Li Anode Protection With the BC Membrane

The use of the BC membrane resulted in an apparent morphological change at the anode. Figure 4a displays the SEM image of the pristine lithium anode, and after the 1st discharge the Li surface becomes rough in the cell with the GF (see Figure 4b), and after 37th discharge the surface is seriously corroded with large and deep cracks as shown in Figure 4c, and

after the 74th discharge the Li metal is depleted into white powders (see Figure 4d), supporting the speculation of the LOB's failure mainly caused by Li depletion as shown in Figure 3d. In the LOB with the BC membrane, the Li surface remains minor change till the 37th discharge (see Figure 4e,f), and after 74th discharge the Li surface turns rough Figure 4g, and after the 341th discharge the Li anode remains structural integrity (see Figure 4h), indicating that the use of the BC membrane effectively protected the Li anode from corrosion by shuttled anions, and Li dendrite growth was effectively suppressed. The dense bacterial cellulose nanofibrous networks provide with tortuous  $\text{Li}^+$  transport paths, leading to the uniform  $\text{Li}^+$  flux in the Li stripping/plating processes, which effectively postpones the depletion of Li anode.

The effect of the BC membrane on anode protection was investigated in comparison with the GF. XRD analysis as illustrated in Supporting Information S1: Figure 12 indicates that the composition of the white powders collected from the Li anode is attributed to LiOH (PDF No. 85-1064). Figure 5 displays the fitting results of the resolved XPS signals of  $\text{Li}_{1s}$  (Figure 5a),  $\text{C}_{1s}$  (Figure 5b) and  $\text{O}_{1s}$  (Figure 5c) of the Li anodes in the cells with the GF and BC membrane. In Figure 5a, the fitted peak at 55.4 eV indicates the presence of  $\text{Li}_2\text{CO}_3$ ,  $\text{RCO}_2\text{CO}_2\text{Li}$  and  $\text{RCH}_2\text{CO}_2\text{Li}$  on the surface of the pristine Li anode. After 10 cycles in the LOB with the GF, two fitted peaks at 55.4 and 54.6 eV, indicating the presence of  $\text{Li}_2\text{CO}_3$ ,  $\text{RCO}_2\text{CO}_2\text{Li}$ ,  $\text{RCH}_2\text{CO}_2\text{Li}$  and LiOH. In contrast, the Li anode in the cell with the BC membrane remains one fitted peak at 55.4 eV, indicating that no LiOH was generated corresponding to the Li corrosion [26]. Figure 5b shows the fitting of the fine spectrum of  $\text{C}_{1s}$  orbit for the pristine Li, where four peaks at 284.8, 289.9, 285.5, and 288.6 eV were obtained assigned to C-C,  $\text{Li}_2\text{CO}_3$ ,  $\text{RCH}_2\text{CO}_2\text{Li}$  and C-O, respectively. Figure 5c shows the fine spectrum of  $\text{O}_{1s}$  orbit, with fitted peak at 531.6 and 533.1 eV corresponding to  $\text{Li}_2\text{CO}_3$  and  $\text{RCH}_2\text{CO}_2\text{Li}$  respectively [23]. After 10 cycles in the LOB with the GF, a new peak of LiOH appears at 531.2 eV. According to XPS analysis of Li surface, the BC membrane absorbs or blocks corrosive substances for Li damage, effectively protects Li, and provides basic protection for LOBs long cycle.

### 3.4 | Cathode Process With the BC Membrane

The use of the BC membrane also optimized the cathode process of LOBs. Electrochemical analysis serves to understand the performance and side reactions in iodide-assisted LOBs. Cyclic voltammograms (CV) in Figure 6a illustrate that the LOB with the BC membrane exhibits larger peaks in both ORR and OER

processes than the cell with the GF. By the assistance of  $\text{I}^-$ , the discharge product can be converted from  $\text{Li}_2\text{O}_2$  to LiOH in ORR process, accompanied with the formation of its oxidized form  $\text{I}_3^-$ . In OER process, the  $\text{I}_3^-$  assists the conversion from LiOH to  $\text{O}_2$ , resulting in the reduction from  $\text{I}_3^-$  to  $\text{I}^-$ . Therefore, the peak currents in the CV profiles associate closely to the local concentration of  $\text{I}^-/\text{I}_3^-$  at the cathode. The BC membrane effectively inhibited the shuttling of  $\text{I}^-$  and  $\text{I}_3^-$  to the anode, and hence the local concentration of  $\text{I}^-/\text{I}_3^-$  at the cathode was kept higher than the GF, leading to larger reduction and oxidation peaks in the CV curves. Supporting Information S1: Figure 13 displays the CV curves after 50th test. The 50th CV curve shows considerably reduced current responses, indicating changes in the electrode over multiple cycles. In LOB with GF, the peaks in both ORR and OER processes nearly disappeared. As comparison, BC membrane still exhibits excellent electrochemical performance and maintains high cycling stability over multiple cycles. Raman analysis of the discharge products of the LOB at the cathode with GF and BC membrane after the first discharge demonstrated that the use of the BC membrane apparently increased the production of LiOH and reversibility of the LOB (see Figure 6b), because of the local higher concentration of  $\text{I}^-/\text{I}_3^-$  at the cathode. Supporting Information S1: Figure 14 displays the Nyquist plot tested in SS||SS symmetrical batteries for the GF and BC membrane, which were taken from the failure LOBs after long-term cycling. It is seen that the impedance of the GF (21.3  $\Omega$ ) becomes apparently larger than the BC-3 membrane (18.1  $\Omega$ ), due to the clogging of by-products in the GF.

Figure 7a shows the SEM image of the pristine MWNTs at the cathode. After the 1st discharge, the MWNTs are coated with discharge product in the LOB with the GF (Figure 7b), where some discharge product remains after the 1st recharge (Figure 7c). After the 74th discharge, MWNTs were fully

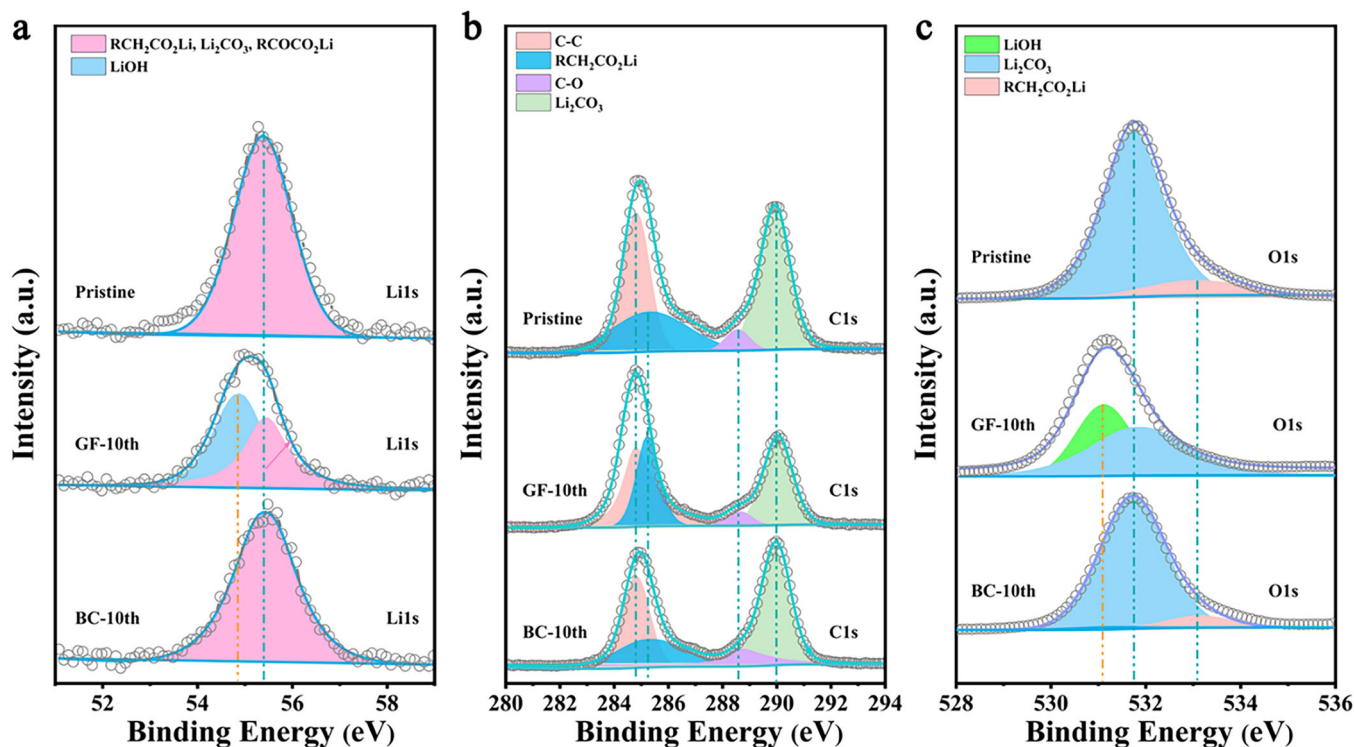
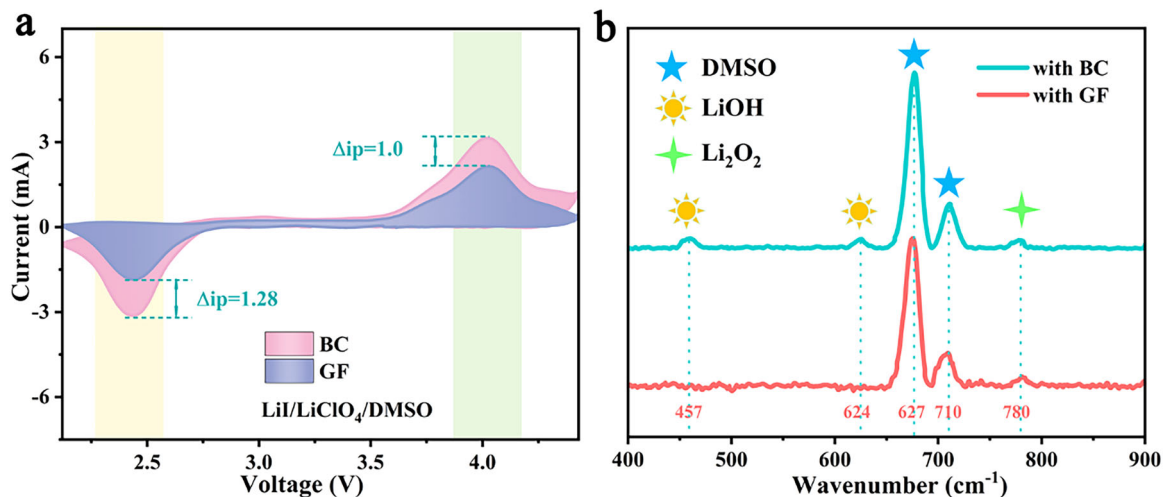
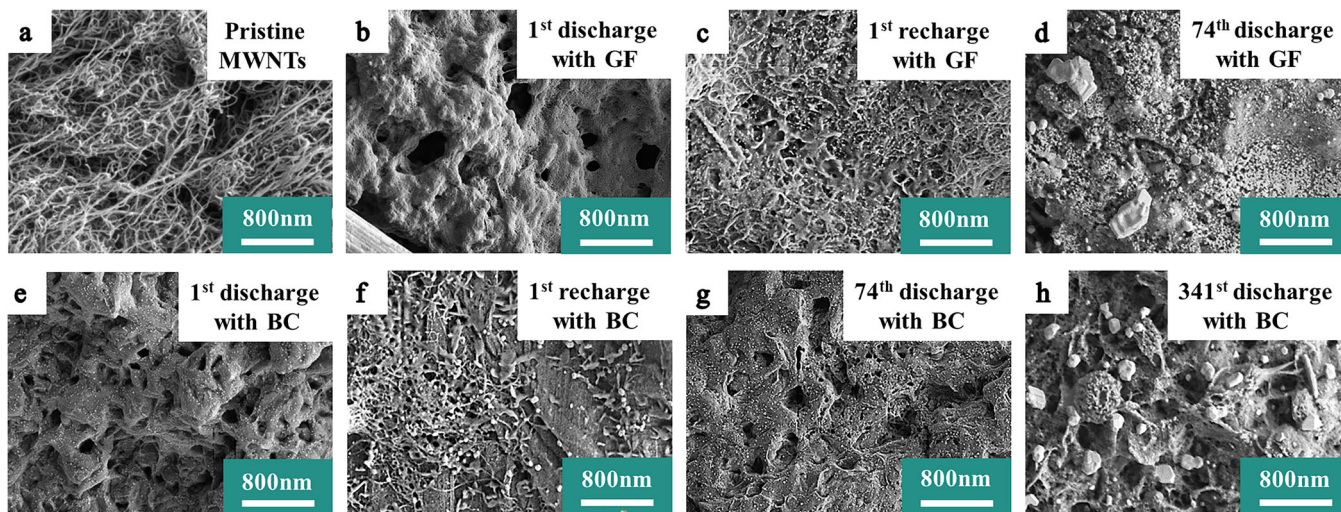


FIGURE 5 | (a-c) Fitting of resolved XPS  $\text{Li}_{1s}$ ,  $\text{C}_{1s}$ ,  $\text{O}_{1s}$  signals for the pristine and cycled anodes in the LOBs with the GF and BC membrane.



**FIGURE 6** | (a) CV in the Li/LiClO<sub>4</sub>/DMSO electrolytes with GF and BC membrane. (b) Raman analysis of the cathode product after the 1st discharge in the LOBs with the GF and BC membrane.



**FIGURE 7** | (a) SEM image of the pristine MWNTs cathode. SEM images of the MWNTs after the (b) 1st discharge; (c) 1st recharge and (d) 74th discharge in the GF cell. SEM of the MWNTs after the (e) 1st discharge; (f) 1st recharge; (g) 74th discharge, and (h) 341th discharge in the BC cell.

covered by large blocks of discharge product (see Figure 7d). In the cell with the BC membrane, Figure 7e shows that after the 1st discharge the MWNTs are covered by film-like discharge product, which was almost completely decomposed after the 1st recharge as depicted in Figure 7f. The MWNTs are still visible after the 74th discharge (see Figure 7g), which are covered by large blocks of discharge product after the 341th discharge (see Figure 7h). Combining with Figure 3d, the charge potential increase associates closely with the accumulation of discharge product at the cathode, which is mainly responsible for the failure of the LOB with the BC membrane.

## 4 | Conclusion

Our work presents a novel BC membrane with ion-selective permeability and was successfully applied to iodine-assisted LOB. The BC membrane significantly outperforms conventional GF in several aspects. The cycle life heightened from 74 to 341 with a current density of 1000 mA g<sup>-1</sup> and a capacity of

1000 mAh g<sup>-1</sup>. Besides, the rate performance raised from 42 to 36 to 215 and 116, respectively, at rates of 3000 and 5000 mA g<sup>-1</sup>. The fully discharged capacity of BC cell extended to 32,310 mAh g<sup>-1</sup>, nearly 7 times more than GF cell (4163 mAh g<sup>-1</sup>). Symmetric cell with the BC membrane exhibited excellent anodic reversibility (almost 800 h). The BC membrane effectively avoided the damaging of I<sup>-</sup>, I<sub>3</sub><sup>-</sup> and other harmful species in the cathode and reserved as a protector of the lithium anode. At the same time, it enhanced the deposition/dissolution of lithium during battery cycle process, and let an iodide-mediated cathodic reaction proceed, which is vital for the optimization of inorganic LOBs system. The BC membrane overcomes the drawbacks inherited from conventional GF, including stabilization available for redox (such as LiI) assisted LOBs.

## Author Contributions

**Aqiang Wu** and **Mingxing Wang**: writing – original draft, validation, investigation, formal analysis, data curation, conceptualization.

**Yaming Pang, Xinyu Li, Xiangqun Zhuge, Zhihong Luo, Guogang Ren, Yurong Ren, Dan Liu, and Weiwei Lei:** writing – original draft, software, data curation, conceptualization. **Kun Luo and Jianwei Lu:** writing – review and editing, supervision, project administration, funding acquisition, conceptualization.

### Acknowledgements

The authors gratefully acknowledge the financial support from the National Natural Science Foundation of China (Nos. 51874051 and 52111530139), the Australian Research Council Discovery Program (DP220103416), and Australian Research Council Future Fellowships (FT200100730 and FT210100804).

### Conflicts of Interest

The authors declare no conflicts of interest.

### Data Availability Statement

The data that support the findings of this study are available on request from the corresponding author. The data are not publicly available due to privacy or ethical restrictions.

### References

1. a) H. Yu, D. Liu, X. Feng, and Y. Zhang, “Recent Progresses, Challenges and Perspectives on Rechargeable Li-O<sub>2</sub> Batteries,” *Nano Select* 1 (2020): 79–93; b) H.-S. Woo, Y.-B. Moon, S. Seo, H.-T. Lee, and D.-W. Kim, “Semi-Interpenetrating Polymer Network Composite Gel Electrolytes Employing Vinyl-Functionalized Silica for Lithium–Oxygen Batteries With Enhanced Cycling Stability,” *ACS Applied Materials & Interfaces* 10 (2017): 687–695; c) J. Yi, S. Guo, P. He, and H. Zhou, “Status and Prospects of Polymer Electrolytes for Solid-State Li–O<sub>2</sub> (air) Batteries,” *Energy & Environmental Science* 10 (2017): 860–884; d) D. Yuan, C. Ji, X. Zhuge, et al., “Organic-Inorganic Interlayer Enabling the Stability of PVDF-HFP Modified Li Metal for Lithium-Oxygen Batteries,” *Applied Surface Science* 613 (2023): 155863.
2. a) Z. Luo, G. Zhu, L. Yin, et al., “A Facile Surface Preservation Strategy for the Lithium Anode for High-Performance Li–O<sub>2</sub> Batteries,” *ACS Applied Materials & Interfaces* 12 (2020): 27316–27326; b) Y. Wang and Y.-C. Lu, “Nonaqueous Lithium–Oxygen Batteries: Reaction Mechanism and Critical Open Questions,” *Energy Storage Materials* 28 (2020): 235–246; c) P. Tan, H. R. Jiang, X. B. Zhu, et al., “Advances and Challenges in Lithium-Air Batteries,” *Applied Energy* 204 (2017): 780–806; d) Y. Fan, Z. Yang, W. Hua, et al., “Functionalized Boron Nitride Nanosheets/Graphene Interlayer for Fast and Long-Life Lithium–Sulfur Batteries,” *Advanced Energy Materials* 7 (2017): 1602380; e) C. Chen, J. Wang, D. Liu, et al., “Functionalized Boron Nitride Membranes With Ultrafast Solvent Transport Performance for Molecular Separation,” *Nature Communications* 9 (2018): 1902.
3. Y. Dou, Z. Xie, Y. Wei, Z. Peng, and Z. Zhou, “Redox Mediators for High-Performance Lithium–Oxygen Batteries,” *National Science Review* 9 (2022): nwac040.
4. a) K. Wu, J. Wang, D. Liu, et al., “Highly Thermoconductive, Thermostable, and Super-Flexible Film by Engineering 1D Rigid Rod-Like Aramid Nanofiber/2D Boron Nitride Nanosheets,” *Advanced Materials* 32 (2020): e1906939; b) Y. Qian, J. Shang, D. Liu, et al., “Enhanced Ion Sieving of Graphene Oxide Membranes via Surface Amine Functionalization,” *Journal of the American Chemical Society* 143 (2021): 5080–5090; c) T. Liu, J. Lu, Z. Chen, et al., “Advances, Mechanisms and Applications in Oxygen Evolution Electrocatalysis of Gold-Driven,” *Chemical Engineering Journal* 496 (2024): 153719.
5. H. D. Lim, H. Song, J. Kim, et al., “Superior Rechargeability and Efficiency of Lithium–Oxygen Batteries: Hierarchical Air Electrode Architecture Combined With a Soluble Catalyst,” *Angewandte Chemie International Edition* 53 (2014): 3926–3931.

6. Y. Chen, S. A. Freunberger, Z. Peng, O. Fontaine, and P. G. Bruce, “Charging a Li–O<sub>2</sub> Battery Using a Redox Mediator,” *Nature Chemistry* 5 (2013): 489–494.
7. X. Gao, Y. Chen, L. Johnson, and P. G. Bruce, “Promoting Solution Phase Discharge in Li–O<sub>2</sub> Batteries Containing Weakly Solvating Electrolyte Solutions,” *Nature Materials* 15 (2016): 882–888.
8. a) B. J. Bergner, A. Schürmann, K. Peppler, A. Garsuch, and J. Janek, “Tempo: A Mobile Catalyst for Rechargeable Li–O<sub>2</sub> Batteries,” *Journal of the American Chemical Society* 136 (2014): 15054–15064; b) D. Sun, Y. Shen, W. Zhang, et al., “A Solution-Phase Bifunctional Catalyst for Lithium–Oxygen Batteries,” *Journal of the American Chemical Society* 136 (2014): 8941–8946.
9. X. Wu, H. Wu, S. Guan, et al., “A Molecular Sieve-Containing Protective Separator to Suppress the Shuttle Effect of Redox Mediators in Lithium-Oxygen Batteries,” *Nano Research* 16 (2023): 9453–9460.
10. W.-J. Kwak, I. Rosy, D. Sharon, et al., “Lithium–Oxygen Batteries and Related Systems: Potential, Status, and Future,” *Chemical Reviews* 120 (2020): 6626–6683.
11. N. Feng, P. He, and H. Zhou, “Enabling Catalytic Oxidation of Li<sub>2</sub>O<sub>2</sub> at the Liquid–Solid Interface: The Evolution of an Aprotic Li–O<sub>2</sub> Battery,” *ChemSuschem* 8 (2015): 600–602.
12. S. H. Lee, J. B. Park, H. S. Lim, and Y. K. Sun, “An Advanced Separator for Li–O<sub>2</sub> Batteries: Maximizing the Effect of Redox Mediators,” *Advanced Energy Materials* 7 (2017): 1602417.
13. a) S. M. Ahn, D. Y. Kim, J. Suk, Y. Kang, H. K. Kim, and D. W. Kim, “Mechanism for Preserving Volatile Nitrogen Dioxide and Sustainable Redox Mediation in the Nonaqueous Lithium–Oxygen Battery,” *ACS Applied Materials & Interfaces* 13 (2021): 8159–8168; b) W.-H. Ryu, F. S. Gittleson, J. M. Thomsen, et al., “Heme Biomolecule as Redox Mediator and Oxygen Shuttle for Efficient Charging of Lithium-Oxygen Batteries,” *Nature Communications* 7 (2016): 12925.
14. a) Y. Li, S. Dong, B. Chen, et al., “Li–O<sub>2</sub> Cell With LiI(3-hydroxypropionitrile)<sub>2</sub> as a Redox Mediator: Insight Into the Working Mechanism of I<sup>–</sup> During Charge in Anhydrous Systems,” *Journal of Physical Chemistry Letters* 8 (2017): 4218–4225; b) W.-J. Kwak, D. Hirshberg, D. Sharon, et al., “Understanding the Behavior of Li–Oxygen Cells Containing LiI,” *Journal of Materials Chemistry A* 3 (2015): 8855–8864; c) W. Zhang, Y. Shen, D. Sun, et al., “Promoting Li<sub>2</sub>O<sub>2</sub> Oxidation via Solvent-Assisted Redox Shuttle Process for Low Overpotential Li–O<sub>2</sub> Battery,” *Nano Energy* 30 (2016): 43–51; d) P. Zhang, B. Han, X. Yang, et al., “Revealing the Intrinsic Atomic Structure and Chemistry of Amorphous LiO<sub>2</sub>-Containing Products in Li–O<sub>2</sub> Batteries Using Cryogenic Electron Microscopy,” *Journal of the American Chemical Society* 144 (2022): 2129; e) T. Liu, M. Leskes, W. Yu, et al., “Cycling Li–O<sub>2</sub> Batteries via LiOH Formation and Decomposition,” *Science* 350 (2015): 530–533.
15. a) Y. Zhao, Y. Ye, F. Wu, Y. Li, L. Li, and R. Chen, “Anode Interface Engineering and Architecture Design for High-Performance Lithium–Sulfur Batteries,” *Advanced Materials* 31 (2019): 1806532; b) L. Fan, M. Li, X. Li, W. Xiao, Z. Chen, and J. Lu, “Interlayer Material Selection for Lithium-Sulfur Batteries,” *Joule* 3 (2019): 361–386; c) T. Tao, S. Lu, Y. Fan, W. Lei, S. Huang, and Y. Chen, “Anode Improvement in Rechargeable Lithium-Sulfur Batteries,” *Advanced Materials* 29 (2017): 1700542; d) J. Zhang, S. Uzun, S. Seyedin, et al., “Additive-Free MXene Liquid Crystals and Fibers,” *ACS Central Science* 6 (2020): 254–265.
16. S. Wu, Y. Qiao, H. Deng, and H. Zhou, “A Single Ion Conducting Separator and Dual Mediator-Based Electrolyte for High-Performance Lithium–Oxygen Batteries With Non-Carbon Cathodes,” *Journal of Materials Chemistry A* 6 (2018): 9816–9822.
17. W. Chen, Z. Luo, X. Zhuge, et al., “Protecting Lithium Anode With Ionic Liquid Modified Poly(Vinylidene Fluoride) Single Ion Conducting Separators for Iodide-Assisted Lithium Oxygen Batteries,” *Journal of Energy Storage* 50 (2022): 104580.

18. Z.-F. Chen, X. Lin, H. Xia, et al., "A Functionalized Membrane for Lithium–Oxygen Batteries to Suppress the Shuttle Effect of Redox Mediators," *Journal of Materials Chemistry A* 7 (2019): 14260–14270.
19. a) Y. Wang, D. Li, S. Zhang, Z. Kang, H. Xie, and J. Liu, "Poly (3,4-Ethylenedioxythiophene):poly (Styrenesulfonate)- Decorated Separator in Li-O<sub>2</sub> Batteries: Suppressing the Shuttle Effect of Dual Redox Mediators by Coulombic Interactions," *Journal of Power Sources* 466 (2020): 228336; b) Y. Qiao, Y. He, S. Wu, et al., "MOF-Based Separator in an Li-O<sub>2</sub> Battery: An Effective Strategy to Restrain the Shuttling of Dual Redox Mediators," *ACS Energy Letters* 3 (2018): 463–468; c) H. Zhang, C. Li, M. Piszcz, et al., "Single Lithium-Ion Conducting Solid Polymer Electrolytes: Advances and Perspectives," *Chemical Society Reviews* 46 (2017): 797–815.
20. a) V. D. Girard, J. Chaussé, and P. Vermette. *Journal of Applied Polymer Science* 141 (2024): e55163; b) P. V. Krasteva, J. Bernal-Bayard, L. Travier, et al., "Insights Into the Structure and Assembly of a Bacterial Cellulose Secretion System," *Nature Communications* 8 (2017): 2065; c) P. Song, J. Dai, G. Chen, et al., "Bioinspired Design of Strong, Tough, and Thermally Stable Polymeric Materials via nanoconfinement," *ACS Nano* 12 (2018): 9266.
21. a) Z. Zhang, Y. Li, X. Cui, et al., "Understanding the Advantageous Features of Bacterial Cellulose-Based Separator in Li-S Battery," *Advanced Materials Interfaces* 10 (2023): 2201730; b) C. Huang, H. Ji, Y. Yang, et al., "Tempo-Oxidized Bacterial Cellulose Nanofiber Membranes as High-Performance Separators for Lithium-Ion Batteries," *Carbohydrate Polymers* 230 (2020): 115570; c) C. Cheng, R. Yang, Y. Wang, D. Fu, J. Sheng, and X. Guo, "A Bacterial Cellulose-Based Separator With Tunable Pore Size for Lithium-Ion Batteries," *Carbohydrate Polymers* 304 (2023): 120489.
22. a) G. Zhang, D. Zhang, R. Yang, et al., "A Multifunctional Wood-Derived Separator Towards the Problems of Semi-Open System in Lithium-Oxygen Batteries," *Advanced Functional Materials* 33 (2023): 2304981; b) R. Gonçalves, E. Lizundia, M. M. Silva, C. M. Costa, and S. Lanceros-Méndez, "Mesoporous Cellulose Nanocrystal Membranes as Battery Separators for Environmentally Safer Lithium-Ion Batteries," *ACS Applied Energy Materials* 2 (2019): 3749–3761.
23. K. Luo, G. Zhu, Y. Zhao, et al., "Enhanced Cycling Stability of Li–O<sub>2</sub> Batteries by Using a polyurethane/SiO<sub>2</sub>/Glass Fiber Nanocomposite Separator," *Journal of Materials Chemistry A* 6 (2018): 7770–7776.
24. M. F. Rosa, E. S. Medeiros, J. A. Malmonge, et al., "Cellulose Nanowhiskers From Coconut Husk Fibers: Effect of Preparation Conditions on Their Thermal and Morphological Behavior," *Carbohydrate Polymers* 81 (2010): 83–92.
25. N. Mittal, A. Ojanguren, N. Cavašin, E. Lizundia, and M. Niederberger, "Transient Rechargeable Battery With a High Lithium Transport Number Cellulosic Separator," *Advanced Functional Materials* 31 (2021): 2101827.
26. H. Mu, K. Luo, Y. Pang, et al., "Mesoporous SiO<sub>2</sub> Anode Armour for Lithium Oxygen Battery," *Chemical Engineering Journal* 475 (2023): 146489.

### Supporting Information

Additional supporting information can be found online in the Supporting Information section.